Journal of Structural Biology 195 (2016) 123–128

Contents lists available at ScienceDirect

Journal of Structural Biology

journal homepage: www.elsevier.com/locate/yjsbi

Local analysis of strains and rotations for macromolecular electron microscopy maps

C.O.S. Sorzano [a,b,*], A. Martín-Ramos [b], F. Prieto [b], R. Melero [a], J. Martín-Benito [a], S. Jonic [c], J. Navas-Calvente [a], J. Vargas [a], J. Otón [a], V. Abrishami [a], J.M. de la Rosa-Trevín [a], J. Gómez-Blanco [a], J.L. Vilas [a], R. Marabini [d], J.M. Carazo [a]

[a] Centro Nac. Biotecnología (CSIC), c/Darwin, 3, 28049 Cantoblanco, Madrid, Spain
[b] Univ. San Pablo – CEU, Campus Urb. Montepríncipe, 28668 Boadilla del Monte, Madrid, Spain
[c] IMPMC, Sorbonne Universités – CNRS UMR 7590, UPMC University Paris 6, MNHN, IRDUMR206, 75005 Paris, France
[d] Univ. Autónoma de Madrid, 28049 Cantoblanco, Madrid, Spain

ARTICLE INFO

Article history:
Received 22 February 2016
Received in revised form 1 April 2016
Accepted 6 April 2016
Available online 19 April 2016

Keywords:
Single particle analysis
Local deformation analysis
Local rotations
Local strains
Elastic registration

ABSTRACT

Macromolecular complexes perform their physiological functions by local rearrangements of their constituents and biochemically interacting with their reaction partners. These rearrangements may involve local rotations and the induction of local strains causing different mechanical efforts and stretches at the different areas of the protein. The analysis of these local deformations may reveal important insight into the way proteins perform their tasks. In this paper we introduce a method to perform this kind of local analysis using Electron Microscopy volumes in a fully objective and automatic manner. For doing so, we exploit the continuous nature of the result of an elastic image registration using B-splines as its basis functions. We show that the results obtained by the new automatic method are consistent with previous observations on these macromolecules.

1. Introduction

Biological macromolecules are intrinsically flexible entities that may adopt a variety of conformations as they perform defined biological functions. At high resolution, these conformational changes can be studied through a detailed analysis of the atomic locations in two different conformational states of the macromolecule. This analysis provides precise information about which areas are stretching, which areas are compressing, and which areas are rotating. However, performing the analysis at the atomic level is not always possible simply because many times structural results produce data that are better treated as 3D maps, as it is the case of many macromolecules solved by Electron Microscopy. Electron Microscopy has shown to be a very powerful tool to analyze different macromolecular discrete (Penczek et al., 2006; Penczek et al., 2006; Leschziner and Nogales, 2007; Scheres et al., 2007; Spahn and Penczek, 2009; Shatsky et al., 2010; Scheres, 2012; Klaholz, 2015) or continuous states (Dashti et al., 2014; Jin et al., 2014). However, given two medium-low resolution conformational states of the macromolecule (in our experimental section we show examples with resolutions ranging from 3.5 Å to 20 Å), an approach to automatically analyse the differences between the maps is not available. The most common action is to perform a morphing (e.g., with Chimera) between the two states so that the researcher gets an idea of the regions of the proteins primarily changing. However, from the video itself it is impossible to know if a certain region is compressing, stretching or simply rotating with respect to its surroundings.

In this article we introduce the first computational tool, to the best of our knowledge, in which the two different kinds of movements (local rotations and local strains) can be separated. The method works at the level of the EM reconstructed maps with the advantage that it can handle a wide variety of resolutions, and the disadvantage that the deformations explored are not stereochemically constrained. The method is based on the differential analysis of the deformation field between two conformational states as calculated with an elastic registration algorithm. Elastic registration is a well-established field in Image Processing in which the correspondence between equivalent coordinates in two different maps is estimated by computational means (Holden, 2008). The term elastic is used as opposed to rigid registration in which only global rotations and translations are allowed. In elastic

* Corresponding author at: Centro Nac. Biotecnología (CSIC), c/Darwin, 3, 28049 Cantoblanco, Madrid, Spain.
E-mail address: coss@cnb.csic.es (C.O.S. Sorzano).

http://dx.doi.org/10.1016/j.jsb.2016.04.001
1047-8477/

registration each part of the images is allowed to move independently, although some regularization may be imposed to constrain the deformation field to be smooth. As we show below, the differential analysis of the local properties of the deformation field allows distinguishing between local strains (compression and stretching) and local rotations. We show in three different experimental cases that our method provides results consistent with the conformational changes described in their corresponding reference publications.

2. Materials and methods

In this section the methodology for the local analysis of structural strains and rotations is described. This theory is well established in Continuum Mechanics and it is here presented in connection with the issue of volume registration as it is employed to identify the deformation field between two volumes. The input to the method is a pair of EM maps describing two different, although similar, states of a given macromolecule. Let us call these maps as $V_0(\mathbf{r})$ and $V_F(\mathbf{r})$, standing for the initial and final state ($\mathbf{r}=(x,y,z)^T\in\mathbb{R}^3$ is the spatial location at which the maps are evaluated). In the following, we assume that any rigid motion between V_0 and V_F has already been removed (in our examples we use Scipion's protocol "align volume", http://scipion.cnb.csic.es, de la Rosa-Trevín et al., 2016). At this stage, we search for a continuous deformation field, $\mathbf{g}(\mathbf{r})=(g_x(\mathbf{r}),g_y(\mathbf{r}),g_z(\mathbf{r}))^T\in\mathbb{R}^3$, that transforms coordinates from the final to the initial state such that

$$V_F(\mathbf{r})\approx V_0(\mathbf{g}(\mathbf{r}))$$

If the initial and the final state were identical, $\mathbf{g}(\mathbf{r})$ would be the identity transformation ($\mathbf{g}(\mathbf{r})=\mathbf{r}$). We define the displacement vector field as

$$\mathbf{u}(\mathbf{r})=\mathbf{g}(\mathbf{r})-\mathbf{r}$$

and at each point we can calculate the displacement gradient as

$$U(\mathbf{r})=\nabla\mathbf{u}(\mathbf{r})=\begin{pmatrix}\frac{\partial g_x}{\partial x}(\mathbf{r})-1 & \frac{\partial g_x}{\partial y}(\mathbf{r}) & \frac{\partial g_x}{\partial z}(\mathbf{r})\\ \frac{\partial g_y}{\partial x}(\mathbf{r}) & \frac{\partial g_y}{\partial y}(\mathbf{r})-1 & \frac{\partial g_y}{\partial z}(\mathbf{r})\\ \frac{\partial g_z}{\partial x}(\mathbf{r}) & \frac{\partial g_z}{\partial y}(\mathbf{r}) & \frac{\partial g_z}{\partial z}(\mathbf{r})-1\end{pmatrix}$$

We may decompose this tensor in its symmetric, $D(\mathbf{r})$, and antisymmetric, $H(\mathbf{r})$, parts (see Sadd (2005) [Chap. 2.1] for more details):

$$D(\mathbf{r})=\tfrac{1}{2}(U(\mathbf{r})+U^T(\mathbf{r}))$$
$$H(\mathbf{r})=\tfrac{1}{2}(U(\mathbf{r})-U^T(\mathbf{r}))$$

such that

$$U(\mathbf{r})=D(\mathbf{r})+H(\mathbf{r})$$

D is a tensor that describes local deformations while H is a tensor that describes local rotations. Note that the D, H decomposition is not the Helmholtz decomposition of a vector field ($\mathbf{u}(\mathbf{r})=\nabla\phi(\mathbf{r})+\nabla\times\boldsymbol{\psi}(\mathbf{r})$), although the D, H decomposition could be calculated from the Helmholtz potentials. The eigenvalues of D describe how the final structure, V_F, is locally deformed (suffering local strains that promote local stretching or compression) to match the initial state, V_0. The sign of the eigenvalue denotes whether there is a compression or a stretching, while its magnitude indicates the strength of the deformation. Similarly, the eigenvalues of H describe local rotations. Note that global rotations have already been taken away and global shifts result in null derivatives (so that they do not appear in the tensor U). We should note that due to the antisymmetric nature of H, its eigenvalues are always of the form 0, $i\alpha$, $-i\alpha$, that is, one of the eigenvalues is always 0, and the other two are purely imaginary, complex conjugates of each other (the larger the local rotation, the larger α).

At each location of the final state, we summarize the information of these two tensors by a local strain and local rotation as

$$\begin{aligned}\text{Local Strain }(\mathbf{r}) &= |\det D(\mathbf{r})|\\ \text{Local Rotation }(\mathbf{r}) &= |\alpha(\mathbf{r})|\end{aligned}$$

If there is no local strain, all eigenvalues of D should be 0. The further these eigenvalues are from 0, the larger the local strain. If an eigenvalue is positive, it means that, locally, the overall effect is a stretching of the molecule. If an eigenvalue is negative, then, locally, the dominant effect is a compression. Note that the determinant is combining the strains in three perpendicular directions, so that there could be compression in one direction and stretching in the other two. The determinant is the multiplication of the three eigenvalues and, consequently, reduces a richer information to a single number that can be easily visualized and interpreted. Similarly, the local rotation should be the local torsion angle in radians.

This local analysis requires knowing the deformation field $\mathbf{g}(\mathbf{r})$. This is a well-known problem in image processing called elastic or non-rigid image registration, and many algorithms exist to solve it (Zitova and Flusser, 2003). Spline descriptions of the deformation field have shown to be very effective in describing rich deformation fields as well as vector field regularizers (Sorzano et al., 2005; Arganda-Carreras et al., 2006; Arganda-Carreras et al., 2008) (see Appendix). Additionally, they allow the analytical calculation at any spatial point of the derivatives needed for the displacement gradient. In this work we consider deformation fields of the form

$$\mathbf{g}(\mathbf{r})=\sum_{jkl}\mathbf{c}_{jkl}\beta_3\left(\frac{\mathbf{r}}{h}-\begin{pmatrix}j\\k\\l\end{pmatrix}\right) \tag{1}$$

where j, k and l are dummy indexes to run over a cubic grid of tensor product splines (see the Appendix for more details), $\mathbf{c}_{jkl}\in\mathbb{R}^3$ is a vector of spline coefficients, h is a scale factor, and $\beta_3(\mathbf{r})$ is the three-dimensional, tensor product spline defined as

$$\beta_3(\mathbf{r})=\beta_3(x)\beta_3(y)\beta_3(z)$$

where $\beta_3(x)$ is the cubic B-spline.

The goal of the image registration problem is to find the coefficients $\mathbf{c}_{jkl}$ such that the initial and final maps are as similar as possible:

$$\underset{\mathbf{c}_{jkl}}{\operatorname{argmin}}\|V_F(\mathbf{r})-V_0(\mathbf{g}(\mathbf{r}))\|^2$$

For this minimization we follow the method described by Myronenko and Song (2010), in which a pyramidal coarse-to-fine approach to the image registration is followed. h is progressively decreased as the pyramid progresses (in our case, we employ three levels of the pyramid, which results in $h=5$, that is, in the finest detail level of the pyramid there is a spline every 5 voxels in each direction, X, Y, Z).

The main two alternatives to describing the deformation field with B-splines are thin-plate splines (Rohr et al., 2004) and pixel-by-pixel defined deformation fields (Guimond et al., 2001). The first approach requires knowledge of corresponding coordinates (that is, pairs of points in the two structures that correspond to the same molecular location), which prevents automating the algorithm since it requires user input. The second approach has proved to be a powerful registration technique, especially for the definition of diffeomorphisms. However, it is not well suited for our purpose since we need to calculate derivatives of the

deformation field and a pixel-valued deformation field is only amenable to numerical differentiation schemes.

3. Results

In the following section, we show how the method performs very well in three different experimental cases. Indeed, we show how the new approach is able to reproduce in a fully automatic manner the manual analysis on map differences reported in the original publication of each one of the examples. We also show how the method effectively separates local rotations from local strains allowing the researcher to give a biological interpretation of each one of the effects.

3.1. Experiment 1: Human mitochondrial ribosome

We focus on the analysis of the human mitochondrial ribosome using the new tools described in this work. The starting data correspond to Class 1 and Class 2 structures as reported by Amunts et al. (2015), accessible as EMDB entries number 2876 and 2877, respectively. As initially described by Amunts et al. (2015), the most obvious relationship between the two classes is that Class 2 is related to Class 1 by a 9.2° ratchet-like rotation of the small subunit around bridge B3. Indeed, this movement is very clearly represented by the analysis of the local rotations that we show in Fig. 1 (top). Colors represent the relative degree of rotation, and it is immediate to realize that the small subunit is very uniformly colored, indicating a close to global rotation of the entire small subunit. Beyond this first observation, the local rotations map indicates strong changes at the level of bridges between the head of the small subunit and the Central Protuberance. The large subunit presents some relatively small additional rotations, all concentrated at the interface between the two subunits. The parallel analysis of local stress nicely complements the one of local rotations. Indeed, the level of local stress at bridges between the head of the small subunit and the Central Protuberance is the most important feature, followed by a relatively small level of stress at discrete sites at the interface between the two subunits (Fig. 1 bottom). It is important to take into consideration that bridges at the head of the small subunit are particularly dynamic among the two structural classes, as indicated by Amunts et al., that is exactly what our analysis is also presenting. Obviously, the structural changes that happen in that area are to be properly modeled considering the structure of the proteins involved and not just in term of their density translation into rotation and stress, but our analysis has identified in an automatic, simple and fast manner those areas in which important structural changes have happened.

3.2. Experiment 2: DnaK-GrpE chaperone complex

In this example we show the analysis of the movement of the GrpE tail in the complex with the chaperone DnaK (Melero et al., 2015). The input volumes were two different conformations of the complex DnaK-GrpE obtained by electron microscopy near to 20 Åresolution (FSC = 0.5). Stated briefly, DnaK chaperone comprises two domains, the nucleotide-binding domain (NBD), responsible for structural and functional changes in the chaperone, and the substrate-binding domain (SBD), involved in substrate interaction. Substrate binding and release is controlled by the nucleotide state, with ATP inducing the open, substrate-receptive state, whereas ADP forces its closure. After the analysis of the EM maps with the method described in this work, the results explain the observations reported in Melero et al. (2015). The local analysis introduced in this work correctly identifies the main movements at the interface between the N-terminal domain of GrpE and the SBD of the chaperone. As depicted in Fig. 2, the results of our method show that the major strains occur in the GrpE N-terminal and the major rotations occur in both, NBD and GrpE N-terminal, in total concordance with the movements proposed by the authors (see Fig. 6 in Melero et al. (2015)).

3.3. Experiment 3: GroEL

In this example we show the ability of the method to analyze sequences of states. For this purpose we studied the conformational changes induced upon the ATP binding to the GroEL chaperonin (Clare et al., 2012). This molecule has a mixture of conformational changes with rigid-body rotations around

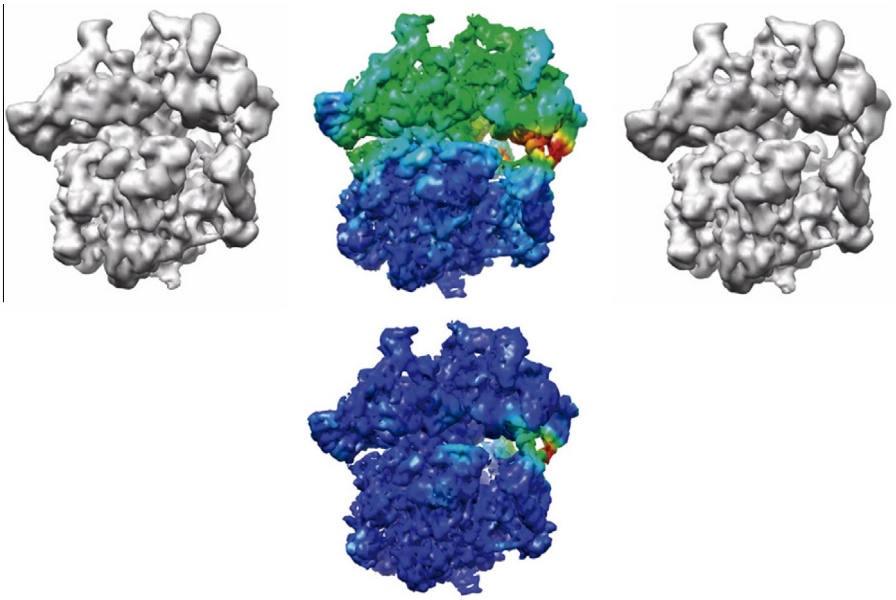

Fig. 1. The human mitochondrial ribosome. Top row: Initial state, V_0, 3D local rotation, and final state, V_F. Bottom row: local strain. Video 1 in the Supplementary Material shows the movement between the two states of this ribosome. The local rotations and strains are represented as colors (from blue, no movement, to red, maximal movement) on the final state, V_F.

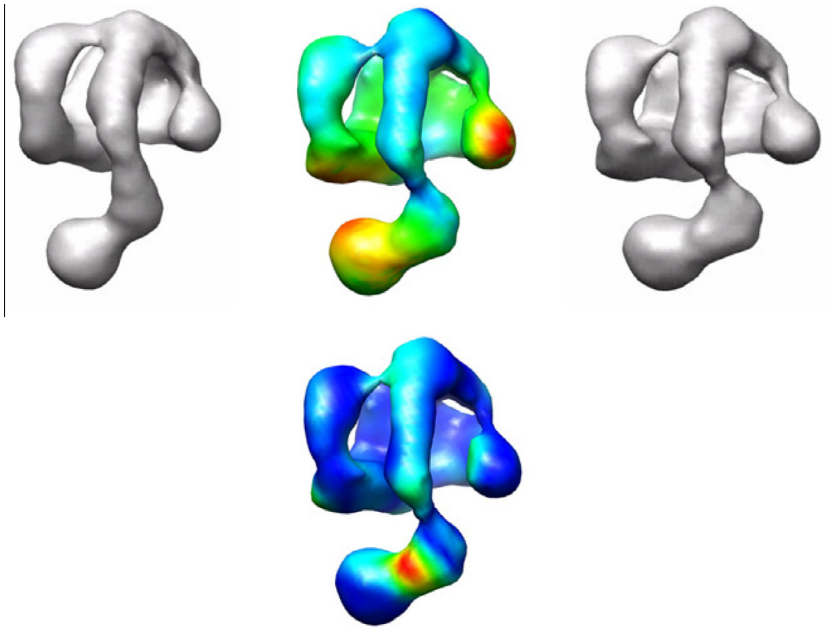

Fig. 2. DnaK-GrpE complex corresponding to classes 1 and 2 in Melero et al. (2015). Top row: Initial state, V_0, 3D local rotation, and final state, V_F. Bottom row: local strain. Video 2 in the Supplementary Material shows the movement between the two states of Dnak-GrpE complex.

determined hinge regions and minor local rearrangements of secondary structure. The input volumes were the different structures determined in presence of ATP, which triggers the conformational changes, following the sequence indicated by Clare et al. (2012). The cooperative binding of the ATP to one ring of the molecule produces conformational changes that affects mainly to the apical domains of that ring, whilst the other ring remains virtually unchanged. As depicted in Fig. 3, the results of our method show that the major rotations and local strains occur in the apical and in the intermediate domains (the top part of the upper ring) in total concordance with the movements proposed by Clare et al. (2012) based on the flexible docking assays performed in the article (see Fig. 2 and Table 1S in Clare et al. (2012)).

4. Discussion and conclusions

In this article we have introduced the first computational method capable of distinguishing between local rotations and local strains (compression or stretching) at the level of medium-low resolution maps. The method is based on the registration of two conformational states of a macromolecule and we have shown that it can successfully be applied to sequence of states. We have also shown that the method is capable of working at different resolutions, not requiring high resolution to perform the analysis. Still, the higher the resolution, the more accurate the registration will be, resulting in a better estimate of the local deformations. The analysis performed surpasses the current standard analysis based

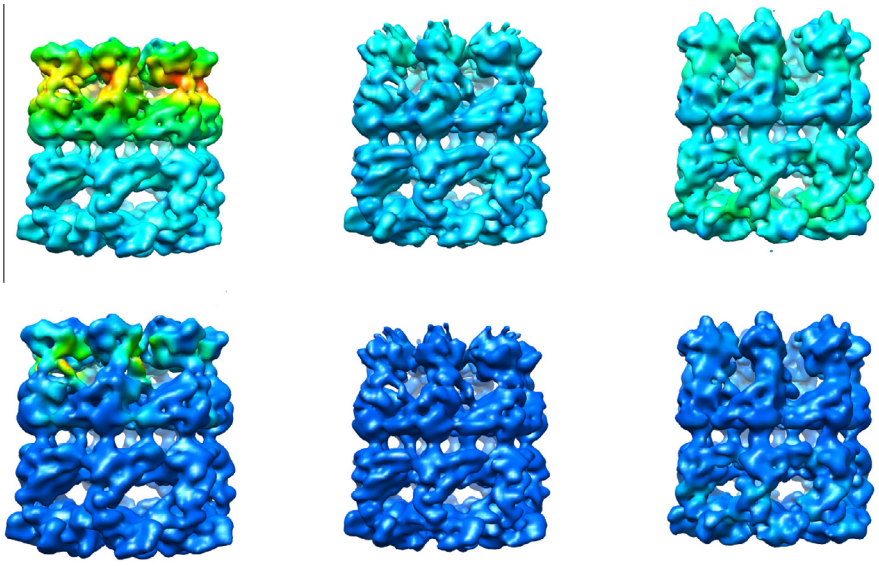

Fig. 3. GroEL conformational changes after ATP binding. The leftmost volumes shows the changes between T:T state and Rs_1:T, the middle volumes the changes between Rs_1:T and Rs_2:T, and the rightmost volumes between Rs_2:T and Rs-open:T. The upper row shows the local rotations and the bottom row the local strains. Videos 3a, 3b and 3c in the Supplmentary Material show the movement between the different states of GroEL.

on morphing between the two states, which only allows to qualitatively assess the properties of the undergoing changes. The method is fully implemented and publicly available in Xmipp (Sorzano et al., 2004; de la Rosa-Trevín et al., 2013) and Scipion (http://scipion.cnb.csic.es) under the name "calculate strain". The calculation core of the method is a Matlab routine, implying that Matlab needs to be installed and accessible from Scipion.

Appendix A. Elastic registration with B-splines

In order to be self-contained let us introduce here the basics of image registration using splines. Image registration is the problem of finding a suitable geometrical transformation, $\mathbf{g}(\mathbf{r})$ that brings two (multidimensional) images, $V_0(\mathbf{r})$ and $V_F(\mathbf{r})$ as close to each other as possible, i.e., the norm of their difference is minimized

$$\underset{\mathbf{g}}{\operatorname{argmin}} \|V_F(\mathbf{r}) - V_0(\mathbf{g}(\mathbf{r}))\|^2$$

If the transformation between the two images is simply a translation $\mathbf{g}(\mathbf{r}) = \mathbf{r} - \mathbf{r}_0$, then the minimization is performed with respect to the only parameter of the transformation, $\mathbf{r}_0$. It is well-known that the solution to this problem can be easily found exploiting the shift property of the Fourier transform. However, we may look for more complicated relationships (rotation, rotation + shift, rotation + shift + scaling + shearing, or rotation + shift + scaling + shearing + mirrors). In general, all these transformation fall under the generic name of affine transformations and they all can be represented by a transformation of the form $\mathbf{g}(\mathbf{r}) = A(\mathbf{r} - \mathbf{r}_0)$ (rigid transformation, i.e., rotations, mirrors and shifts is a subset of affine transformations). The minimization must be done now on A and $\mathbf{r}_0$. Affine transformations preserve parallel lines (if two lines are parallel, their transformed lines are also parallel), although in general, they do not preserve the angles between intersecting lines (rigid transformations preserve the angles of any two lines in the original image). If V_0 and V_F are three-dimensional, as is our case, we have a total of 12 parameters to optimize (9 for the 3×3 A matrix and 3 for $\mathbf{r}_0$).

We may construct even richer transformations. A very common way is to do so by using tensor-product B-splines as shown in Eq. 1 that allow us to express non-rigid transformations as shown in Fig. 4. At this point we may use a less compact notation to add insight into the mathematical properties of this deformation field:

$$\mathbf{g}(\mathbf{r}) = \begin{pmatrix} g_x(\mathbf{r}) \\ g_y(\mathbf{r}) \\ g_z(\mathbf{r}) \end{pmatrix} = \begin{pmatrix} \sum_{jkl} c_{x,jkl} \beta_3\left(\frac{x}{h} - j\right) \beta_3\left(\frac{y}{h} - k\right) \beta_3\left(\frac{z}{h} - l\right) \\ \sum_{jkl} c_{y,jkl} \beta_3\left(\frac{x}{h} - j\right) \beta_3\left(\frac{y}{h} - k\right) \beta_3\left(\frac{z}{h} - l\right) \\ \sum_{jkl} c_{z,jkl} \beta_3\left(\frac{x}{h} - j\right) \beta_3\left(\frac{y}{h} - k\right) \beta_3\left(\frac{z}{h} - l\right) \end{pmatrix} \quad (2)$$

where $c_{x,jkl}$ is the jklth coefficient in the x direction and similarly for $c_{y,jkl}$ and $c_{z,jkl}$. $\beta_3(\chi)$ is the cubic B-spline (see Fig. 5) defined as (Jonic and Sorzano, 2011)

$$\beta_3(\chi) = \begin{cases} \frac{2}{3} + \frac{1}{2}|\chi|^2(|\chi| - 2) & 0 \leqslant |\chi| < 1 \\ \frac{1}{6}(2 - |\chi|^3) & 1 \leqslant |\chi| < 2 \\ 0 & 2 \leqslant |\chi| \end{cases}$$

The terms $\beta_3\left(\frac{x}{h} - j\right)$ shifts the spline to jh and widens the function by a factor h as can be seen in Fig. 5. The parameters to fit the geometrical transformation are the $c_{x,jkl}$, $c_{y,jkl}$ and $c_{z,jkl}$ parameters (normally defined from $i = -1, 0, 1, \ldots, N_x$, $j = -1, 0, 1, \ldots, N_y$ and $k = -1, 0, 1, \ldots, N_z$ being $N_x = \lfloor \frac{X_{dim}}{h} \rfloor + 1$, $N_y = \lfloor \frac{Y_{dim}}{h} \rfloor + 1$, $N_z = \lfloor \frac{Z_{dim}}{h} \rfloor + 1$ and X_{dim}, Y_{dim}, Z_{dim} the X, Y, Z dimensions of V_0 and V_F). Interestingly, B-splines can be used to construct multiresolution approaches using what is called spline pyramids (Unser et al., 1993; Jonic and Sorzano, 2011). The idea is to construct first an approximation to the function $\mathbf{g}$ with a given step h, then this approximation is refined by setting the step to $h/2$ and adding more coefficients (which are initialized from the coefficients calculated for the step h). Additional pyramid levels set the step to $h/4$, $h/8, \ldots$

Interestingly, the derivative of functions defined with B-splines can be analytically calculated by exploiting the property

$$\frac{d\beta_3}{dx}(x) = \beta_2\left(x + \frac{1}{2}\right) - \beta_2\left(x - \frac{1}{2}\right)$$

where β_2 is the quadratic B-spline

$$\beta_2(\chi) = \begin{cases} \frac{3}{4} - |\chi|^2 & 0 \leqslant |\chi| < \frac{1}{2} \\ \frac{1}{2}\left(|\chi| - \frac{3}{2}\right)^2 & \frac{1}{2} \leqslant |\chi| < \frac{3}{2} \\ 0 & \frac{3}{2} \leqslant |\chi| \end{cases}$$

For instance

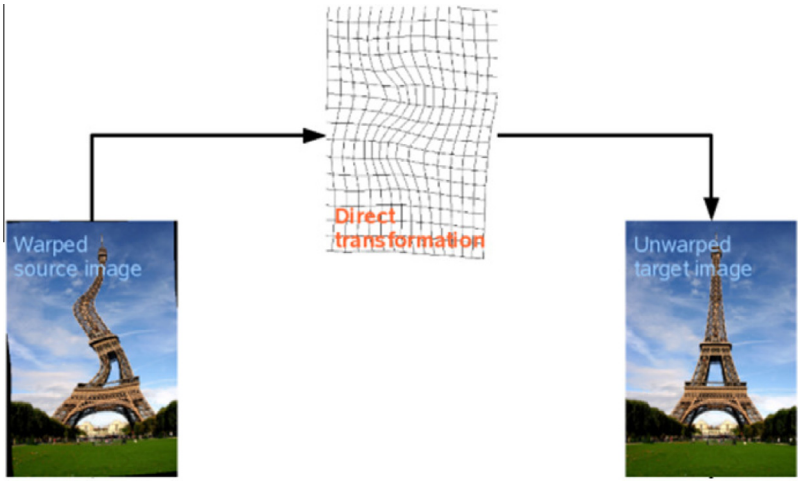

Fig. 4. Example of non-rigid transformation.

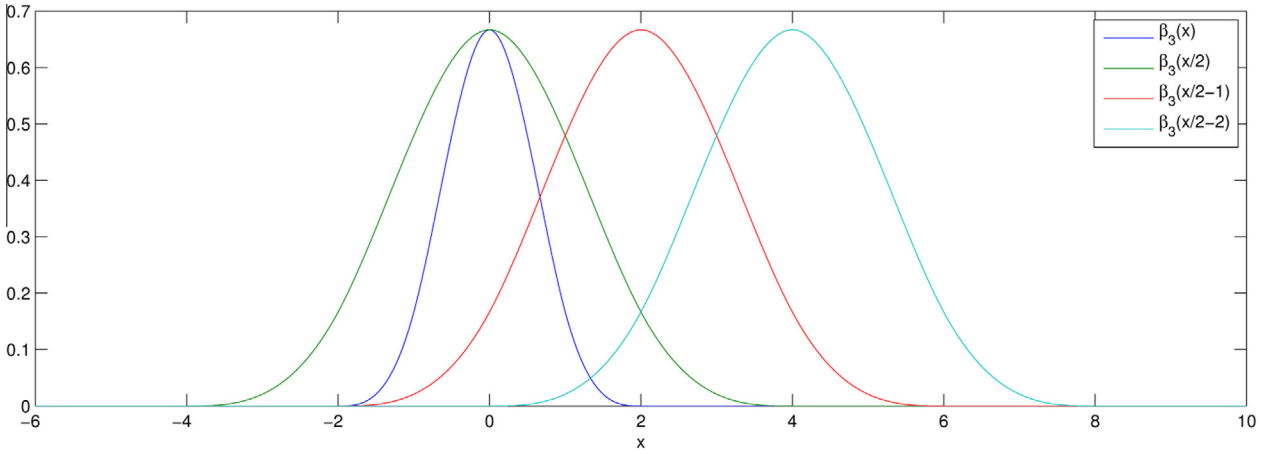

Fig. 5. Cubic B-spline.

$$\frac{\partial}{\partial x}\left(\sum_{jkl} c_{x,jkl}\beta_3\left(\frac{x}{h}-j\right)\beta_3\left(\frac{y}{h}-k\right)\beta_3\left(\frac{z}{h}-l\right)\right) = \sum_{jkl}\frac{c_{x,jkl}}{h}\left(\beta_2\left(\frac{x}{h}-j+\frac{1}{2}\right)-\beta_2\left(\frac{x}{h}-j-\frac{1}{2}\right)\right)\beta_3\left(\frac{y}{h}-k\right)\beta_3\left(\frac{z}{h}-l\right) \quad (3)$$

Appendix B. Supplementary data

Supplementary data associated with this article can be found, in the online version, at http://dx.doi.org/10.1016/j.jsb.2016.04.001.

References

Amunts, A., Brown, A., Toots, J., Scheres, S.H., Ramakrishnan, V., 2015. The structure of the human mitochondrial ribosome. Science 348 (6230), 95–98.

Arganda-Carreras, I., Sorzano, C.O.S., Marabini, R., Carazo, J.M., Ortiz-de Solórzano, C., Kybic, J., 2006. Consistent and elastic registration of histological sections using vector-spline regularization. Lect. Notes Comput. Sci. 4241, 85–95.

Arganda-Carreras, I., Sorzano, C.O.S., Kybic, J., Ortiz de Solórzano, C., 2008. bUnwarpJ: Consistent and elastic registration in imageJ. Methods and applications. Proc. Conference ImageJ Users-Developers, Luxembourg.

Clare, D.K., Vasishtan, D., Stagg, S., Quispe, J., Farr, G.W., Topf, M., Horwich, A.L., Saibil, H.R., 2012. Atp-triggered conformational changes delineate substrate-binding and -folding mechanics of the GroEL chaperonin. Cell 149 (1), 113–123.

Dashti, A., Schwander, P., Langlois, R., Fung, R., Li, W., Hosseinizadeh, A., Liao, H.Y., Pallesen, J., Sharma, G., Stupina, V.A., Simon, A.E., Dinman, J.D., Frank, J., Ourmazd, A., 2014. Trajectories of the ribosome as a Brownian nanomachine. Proc. Natl. Acad. Sci. USA 111 (49), 17492–17497.

de la Rosa-Trevín, J.M., Quintana, A., del Cano, L., Zaldívar, A., Foche, I., Gutiérrez, J., Gómez-Blanco, J., Burguet-Castell, J., Cuenca-Alba, J., Abrishami, V., Vargas, J., Otón, J., Sharov, G., Vilas, J.L., Navas, J., Conesa, P., Kazemi, M., Marabini, R., Sorzano, C.O.S., Carazo, J.M., 2016. Scipion: a software framework toward integration, reproducibility and validation in 3D electron microscopy. J. Struct. Biol. 195 (1), 93–99.

de la Rosa-Trevín, J.M., Otón, J., Marabini, R., Zaldívar, A., Vargas, J., Carazo, J.M., Sorzano, C.O.S., 2013. Xmipp 3.0: an improved software suite for image processing in electron microscopy. J. Struct. Biol. 184 (2), 321–328.

Guimond, A., Roche, A., Ayache, N., Meunier, J., 2001. Three-dimensional multimodal brain warping using demons algorithm and adaptive intensity corrections. IEEE Trans. Med. Imaging 20, 58–69.

Holden, M., 2008. A review of geometric transformations for nonrigid body registration. IEEE Trans. Med. Imaging 27, 111–128.

Jin, Q., Sorzano, C.O.S., de la Rosa-Trevín, J.M., Bilbao-Castro, J.R., Núñez-Ramírez, R., Llorca, O., Tama, F., Jonić, S., 2014. Iterative elastic 3D-to-2D alignment method using normal modes for studying structural dynamics of large macromolecular complexes. Structure 22 (3), 496–506.

Jonic, S., Sorzano, C.O.S., 2011. Splines in biomedical image processing. Opt. Digital Image Process.: Fundam. Appl., 119–134

Klaholz, B.P., 2015. Structure sorting of multiple macromolecular states in heterogeneous cryo-em samples by 3D multivariate statistical analysis. Open J. Stat. 5 (07), 820–836.

Leschziner, A.E., Nogales, E., 2007. Visualizing flexibility at molecular resolution: analysis of heterogeneity in single-particle electron microscopy reconstructions. Ann. Rev. Biophys. Biomol. Struct. 36, 43–62.

Melero, R., Moro, F., Pérez-Calvo, M.Á., Perales-Calvo, J., Quintana-Gallardo, L., Llorca, O., Muga, A., Valpuesta, J.M., 2015. Modulation of the chaperone DnaK allosterism by the nucleotide exchange factor GrpE. J. Biol. Chem. 290 (16), 10083–10092.

Myronenko, A., Song, X., 2010. Intensity-based image registration by minimizing residual complexity. IEEE Trans. Med. Imaging 29 (11), 1882–1891.

Penczek, P.A., Frank, J., Spahn, C.M., 2006. A method of focused classification, based on the bootstrap 3D variance analysis, and its application to EF-G-dependent translocation. J. Struct. Biol. 154, 184–194.

Penczek, P.A., Yang, C., Frank, J., Spahn, C.M., 2006. Estimation of variance in single-particle reconstruction using the bootstrap technique. J. Struct. Biol. 154, 168–183.

Rohr, K., Cathier, P., Worz, S., 2004. Elastic registration of electrophoresis images using intensity information and point landmarks. Pattern Recognit. 37, 1035–1048.

Sadd, M.H., 2005. Elasticity: Theory, Applications, and Numerics. Academic Press.

Scheres, S.H.W., 2012. A Bayesian view on cryo-EM structure determination. J. Mol. Biol. 415 (2), 406–418.

Scheres, S.H.W., Gao, H., Valle, M., Herman, G.T., Eggermont, P.P.B., Frank, J., Carazo, J.M., 2007. Disentangling conformational states of macromolecules in 3D-EM through likelihood optimization. Nat. Methods 4 (1), 27–29.

Shatsky, M., Hall, R.J., Nogales, E., Malik, J., Brenner, S.E., 2010. Automated multi-model reconstruction from single-particle electron microscopy data. J. Struct. Biol. 170 (1), 98–108.

Sorzano, C.O.S., Marabini, R., Velázquez-Muriel, J., Bilbao-Castro, J.R., Scheres, S.H. W., Carazo, J.M., Pascual-Montano, A., 2004. XMIPP: a new generation of an open-source image processing package for electron microscopy. J. Struct. Biol. 148, 194–204.

Sorzano, C.O.S., Thévenaz, P., Unser, M., 2005. Elastic registration of biological images using vector-spline regularization. IEEE Trans. Biomed. Eng. 52, 652–663.

Spahn, C.M.T., Penczek, P.A., 2009. Exploring conformational modes of macromolecular assemblies by multiparticle cryo-EM. Curr. Opin. Struct. Biol. 19 (5), 623–631.

Unser, M., Aldroubi, A., Eden, M., 1993. The L_2 polynomial spline pyramid. IEEE Trans. Pattern Anal. Mach. Intell. 15, 364–378.

Zitova, B., Flusser, J., 2003. Image registration methods: a survey. Image Vis. Comput. 21, 977–1000.